

# Optimizing the Network Topology of a Linear Reservoir Computer

Sahand Tangerami<sup>a</sup>, Nicholas A. Mecholsky<sup>b</sup>, Francesco Sorrentino<sup>c</sup>

<sup>a</sup>*K. N. Toosi University of Technology, Tehran, Iran*

<sup>b</sup>*Catholic University of America, Washington, D.C., United States*

<sup>c</sup>*University of New Mexico, Albuquerque, NM 87131, United States*

---

## Abstract

Machine learning has become a fundamental approach for modeling, prediction, and control, enabling systems to learn from data and perform complex tasks. Reservoir computing is a machine learning tool that leverages high-dimensional dynamical systems to efficiently process temporal data for prediction and observation tasks. Traditionally, the connectivity of a reservoir computer (RC) is generated at random, lacking a principled design. Here, we focus on optimizing the topology of a linear RC to improve its performance and interpretability, which we achieve by decoupling the RC dynamics into a number of independent modes. We then proceed to optimize each one of these modes to perform a given task, which corresponds to selecting an optimal RC connectivity in terms of a given set of eigenvalues of the RC adjacency matrix. Simulations on networks of varying sizes show that the optimized RC significantly outperforms randomly constructed reservoirs in both the training and testing phases and also often surpasses nonlinear reservoirs of comparable size. This approach provides both practical performance advantages and theoretical guidelines for designing efficient, task-specific, and analytically transparent RC architectures.

**Keywords:** Machine learning, networks, optimization, reservoir computer.

---

## 1. Introduction

Machine learning has emerged as a key approach for modeling and control, allowing systems to extract patterns from data and perform complex tasks with high accuracy Zhao et al. (2024); Bensoussan et al. (2022); Hashemi et al. (2023). However, training in many machine learning can be computationally demanding. Reservoir computing, a machine learning tool within the broader class of recurrent neural networks, addresses this challenge by keeping the internal reservoir connectivity fixed and training only the readout layer Jaeger (2001). This allows to perform training in terms of a simple regression operation, as opposed to the more computationally intensive back-propagation. RC has shown to be highly successful in processing temporal and sequential data, especially in prediction and observation tasks McCreesh and Cortés (2024); Shen et al. (2025); Pathak et al. (2018); Jordanou et al. (2022).

In typical implementations, reservoir computers employ nonlinear node dynamics, and their network topologies are chosen at random Yan et al. (2024). Although this random construction often yields satisfactory results in many tasks, it lacks a principled foundation and is not explicitly optimized to perform given tasks of interest Dale et al. (2021). Furthermore, the presence of nonlinearities complicates the analysis of the internal dynamics, making it difficult to characterize key properties such as memory capacity, stability, and input-output relationships. Metzner et al. (2025); Sugiura et al. (2024). Consequently, nonlinear RC often function as black boxes, providing limited insight into how information is processed or stored. In contrast, linear reservoir computing (LRC) significantly improves interpretability and analytical tractability Gauthier et al. (2021). Although linear reservoirs may exhibit lower performance in general, they can be highly effective for tasks with well-understood linear or frequency-driven structures, offering a valuable platform for developing theory-guided, efficient, and generalizable RC systems. Our approach in this paper adopts linear reservoir dynamics, which allows systematic optimization of the network topology to enhance performance on specific tasks of interest.

In what follows, we consider an LRC performing an observation task, in which the reservoir is trained to reconstruct an output signal from knowledge of an input signal Lu et al. (2017). Our objective is to optimize the network topology of the LRC, based on knowledge of the spectral characteristics of the input and output signals. Specifically,

we formulate an optimization problem to determine the optimal set of eigenvalues of the matrix that provides the connectivity between reservoir nodes, which we show leads to a drastic reduction of the training error. By leveraging frequency-domain insights, we identify reservoir topologies that maximize performance and interpretability. Our results show that the optimized LRC not only outperforms randomly constructed LRC but also achieves better performance than nonlinear RC of comparable size.

## 2. System Model and Reservoir Dynamics

We take two signals which we know to be dynamically related to one another,  $\hat{u}(t)$  and  $\hat{y}(t)$ . Fundamentally, our goal is to ‘observe’ or ‘learn’  $\hat{y}(t)$  from knowledge of  $\hat{u}(t)$ . To this end, we extract a set of  $K$  dominant frequencies that are simultaneously present in both  $\hat{y}(t)$  and  $\hat{u}(t)$ , and construct the signals  $y(t)$  and  $u(t)$  that only contain those frequencies Butschek et al. (2022). Hence,  $u(t)$  and  $y(t)$  can be expressed as:

$$u(t) = \sum_{k=1}^K a_k \cos(\omega_k t) \quad (1)$$

$$y(t) = \sum_{k=1}^K b_k \cos(\omega_k t + \phi_k). \quad (2)$$

where  $\{\omega_k\}$  is a set of distinct frequencies,  $a_k$  and  $b_k$  are amplitudes, and  $\phi_k$  are the phases of the training signal with respect to the input signal. We then opt for the simpler problem of learning the training signal  $y(t)$  from knowledge of the input signal  $u(t)$ .

To this end, we introduce a linear reservoir computer, which obeys the dynamics,

$$\dot{\mathbf{r}}(t) = \gamma [-\mathbf{r}(t) + A\mathbf{r}(t) + \mathbf{d}u(t)], \quad (3)$$

where  $\mathbf{r}(t) = [r_1(t), r_2(t), \dots, r_N(t)]$  is the vector of nodes’ readout,  $\gamma$  is a positive constant, the symmetric matrix  $A$  is the reservoir’s adjacency matrix, i.e.,  $A_{ij} = A_{ji}$  describes the strength of the coupling between node  $j$  to node  $i$ , the mask vector  $\mathbf{d} = [d_1, d_2, \dots, d_N]$ ,  $N$  is the number of nodes, and  $u(t)$  is the input signal. We also assume that the matrix  $A$  is Hurwitz, and therefore the reservoir dynamics (3) is stable.

To compute the reservoir modes, the training signal is discretized using a time step  $\tau$ . The reservoir produces an estimate of the training signal, the fit signal  $\check{\mathbf{y}}$ , in terms of a linear combination of the readout matrix  $\Omega_r$  in the coefficient vector,  $\boldsymbol{\kappa}$

$$\Omega_r \boldsymbol{\kappa} = \check{\mathbf{y}}, \quad (4)$$

where

$$\Omega_r = \begin{pmatrix} r_1(\tau) & r_2(\tau) & \dots & r_N(\tau) & 1 \\ r_1(2\tau) & r_2(2\tau) & \dots & r_N(2\tau) & 1 \\ \vdots & \vdots & \vdots & \vdots & \vdots \\ r_1(T\tau) & r_2(T\tau) & \dots & r_N(T\tau) & 1 \end{pmatrix} \quad (5)$$

and  $T$  is the number of time steps. We wish to choose the coefficients of the vector  $\boldsymbol{\kappa}$  that minimizes the error  $\epsilon_r$ ,

$$\epsilon_r = \frac{1}{\sqrt{T}} \|\Omega_r \boldsymbol{\kappa} - \mathbf{y}\|, \quad (6)$$

where  $\|\cdot\|$  denotes the  $L_2$  norm. We compute  $\boldsymbol{\kappa}^* = \Omega_r^\dagger \mathbf{y}$  the optimal vector of the output weights that minimizes  $\epsilon_r$  in Eq. (6), where  $\Omega_r^\dagger = (\Omega_r^T \Omega_r + \beta I)^{-1} \Omega_r^T$  and  $\beta \geq 0$  is the ridge regression parameter Wyffels et al. (2008).

To facilitate optimization of the linear reservoir, we employ modal decomposition to transform the reservoir dynamics into independent modes that can be individually tuned. To do so, since the matrix  $A$  is symmetric, it can be diagonalized as  $A = V\Lambda V^T$ , where  $V$  is an orthogonal matrix whose columns are the eigenvectors of  $A$  and  $\Lambda$  is a diagonal matrix with the real eigenvalues of  $A$  along its main diagonal. We pre-multiply both sides of Eq. (3) by  $V^T$ , and by defining  $\mathbf{q}(t) = V^T \mathbf{r}(t)$  and  $\mathbf{c} = V^T \mathbf{d}$ , the system transforms into the following form,

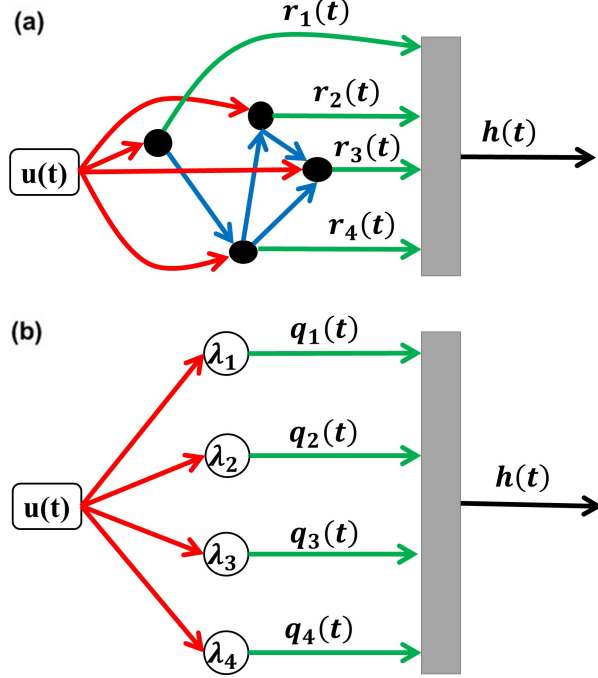


Figure 1: Two equivalent RC network topologies. a) A coupled reservoir computer. b) A decoupled reservoir computer.

$$\dot{\mathbf{q}}(t) = \gamma [-\mathbf{q}(t) + \Lambda \mathbf{q}(t) + \mathbf{c}u(t)], \quad (7)$$

where  $\mathbf{q}$  is the vector of the decoupled reservoir readouts, which breaks up into a set of  $N$  independent modes,

$$\dot{q}_i(t) = \gamma(\lambda_i - 1)q_i(t) + \gamma c_i u(t), \quad i = 1, \dots, N, \quad (8)$$

where  $\lambda_i$  are the eigenvalues of the reservoir's adjacency matrix  $A$ .

Equations (7) and (8) provide a modal decomposition for the reservoir dynamics. The implications of the modal decomposition of an RC are significant and are illustrated in Fig. 1. Panel (a) of this figure shows a coupled reservoir, where nodes are interconnected, whereas panel (b) illustrates a decoupled reservoir computer, in which the reservoir is decomposed into independent modes without node-to-node connections. In particular, the fact that an RC can be decomposed into a number of independent modes (see Fig. 1) has important implications and arguably several advantages in terms of RC robustness, scalability, repurposability, and interoperability. Another fundamental advantage is the possibility of more easily optimizing the structure of a reservoir, as it reduces the parameter space over which the optimization is performed from  $N^2$  entries of the matrix  $A$  to only  $N$  eigenvalues. This is specifically what we do in this paper.

The solution of Eq. (8), is given by,

$$q_i(t) = \exp(\gamma(\lambda_i - 1)t)q_i(0) + \gamma c_i \int_0^t \exp(\gamma(\lambda_i - 1)(t - \tau))u(\tau) d\tau \quad (9)$$

where the first term on the left-hand side of (9) is the free evolution, which by the assumption of stable reservoir dynamics goes to zero for large  $t$ . For large  $t$ , each mode  $q_i$  differs from the others through the coefficient  $\lambda_i$ , while the particular modal amplitude is given by  $c_i$ .

The decoupled reservoir is easier to handle since it consists of independent rather than dependent modes. An important step is to understand the error relationship between the coupled reservoir of Eqs. (3) and the decoupled reservoir of Eqs. (7). This relationship is formally established in Theorem 1.

**Theorem 1.** *Let a coupled linear reservoir and a decoupled linear reservoir be described by Eqs. (3) and (7), respectively. Then, the best-fit signals for the two problems are identical.*

*Proof.* The detailed proof is provided in Appendix I.  $\square$

Since the decoupled reservoir is simpler to work with and it yields the same training and testing errors as the coupled reservoir, in the remainder of the paper we focus on the decoupled reservoir model. Notwithstanding the benefits of the decoupled reservoir, the dimension of the reservoir mode matrix remains large, as it scales with the number of time steps. This dimension can be significantly reduced by transforming the problem into the frequency domain, where the matrix size depends only on the number of input frequencies, which is considerably smaller than the number of time steps. To this end, we reformulate the problem in the frequency domain by applying the Laplace transform to each mode and expressing it through its corresponding transfer function. The transfer function of each mode in Eq. (9) can be expressed as follows.

$$T_i(j\omega) = \frac{\gamma c_i}{j\omega - \gamma(\lambda_i - 1)}. \quad (10)$$

### 2.1. Generic Relation Between the Error In The Time and the Frequency Domain

If we remove the transient component, which corresponds to the first term on the right-hand side of Eq. (9), the time-domain solution for the dynamics of each node in the decoupled reservoir is given by:

$$q_i(t) = \sum_{k=1}^K a_k M_{ik} \cos(\omega_k t + \theta_{ik}) \quad (11)$$

where  $a_k$  denotes the amplitude of the input signal,  $\omega_k$  is the common frequency between the input and output signals,  $M_{ik}$  and  $\theta_{ik}$  represent the magnitude and phase of the reservoir, respectively, which are computed as follows:

$$\begin{aligned} M_{ik} &= \left| \frac{\gamma c_i}{j\omega_k - \gamma(\lambda_i - 1)} \right| = \frac{\gamma |c_i|}{\sqrt{\omega_k^2 + \gamma^2(\lambda_i - 1)^2}} \\ \angle \theta_{ik} &= \angle \frac{\gamma c_i}{j\omega_k - \gamma(\lambda_i - 1)} = \tan^{-1} \left( \frac{\omega_k}{-\gamma(\lambda_i - 1)} \right) \end{aligned} \quad (12)$$

The reservoir state matrix associated with Eq. (11) is:

$$\Omega_q = \begin{bmatrix} q_1(1) & q_2(1) & \dots & q_N(1) \\ q_1(2) & q_2(2) & \dots & q_N(2) \\ \vdots & \vdots & \ddots & \vdots \\ q_1(T) & q_2(T) & \dots & q_N(T) \end{bmatrix} \quad (13)$$

Next, we take the Laplace transform of Eq. (11) and perform an alternative regression in the frequency domain. We note that the expression of Eq. (11) can be interpreted as a linear combination of a set of basis functions, analogous to the representation of a vector in terms of its components. In this context, the basis functions—or *primitives*—are given by  $\{\cos(\omega_1 t + \theta_{11}), \cos(\omega_2 t + \theta_{12}), \dots, \cos(\omega_K t + \theta_{1K})\}$  and the corresponding coefficients for  $q_1(t)$  are  $\{a_1 M_{11}, a_2 M_{12}, \dots, a_K M_{1K}\}$ .

The output of the reservoir computer is constructed as a linear combination of the internal states, referred to as the readouts. By taking the Laplace transform of Eq. (11), we obtain,

$$Q_i(s) = \sum_{k=1}^K a_k M_{ik} \left[ \cos(\theta_{ik}) \frac{s}{s^2 + \omega_k^2} - \sin(\theta_{ik}) \frac{\omega_k}{s^2 + \omega_k^2} \right] \quad (14)$$

Thus the linear combination of  $Q_1(s), Q_2(s), \dots, Q_N(s)$  is equal to,

$$\begin{aligned} \sum_{i=1}^N \tilde{\kappa}_i Q_i(s) &= \sum_{k=1}^K \sum_{i=1}^N a_k \left[ \tilde{\kappa}_i M_{ik} \cos(\theta_{ik}) \frac{s}{s^2 + \omega_k^2} \right] - \sum_{k=1}^K \sum_{i=1}^N a_k \left[ \tilde{\kappa}_i M_{ik} \sin(\theta_{ik}) \frac{\omega_k}{s^2 + \omega_k^2} \right] \\ &= \sum_{k=1}^K \sum_{i=1}^N a_k \left[ \tilde{\kappa}_i M_{ik} \cos(\theta_{ik}) \frac{s}{s^2 + \omega_k^2} - \tilde{\kappa}_i M_{ik} \sin(\theta_{ik}) \frac{\omega_k}{s^2 + \omega_k^2} \right] \end{aligned} \quad (15)$$

$$\tilde{\Omega}_q = \begin{pmatrix} a_1 M_{11} \cos(\theta_{11}) & a_1 M_{21} \cos(\theta_{21}) & \cdots & a_1 M_{N1} \cos(\theta_{N1}) \\ a_1 M_{11} \sin(\theta_{11}) & a_1 M_{21} \sin(\theta_{21}) & \cdots & a_1 M_{N1} \sin(\theta_{N1}) \\ a_2 M_{12} \cos(\theta_{12}) & a_2 M_{22} \cos(\theta_{22}) & \cdots & a_2 M_{N2} \cos(\theta_{N2}) \\ a_2 M_{12} \sin(\theta_{12}) & a_2 M_{22} \sin(\theta_{22}) & \cdots & a_2 M_{N2} \sin(\theta_{N2}) \\ \vdots & \vdots & \ddots & \vdots \\ a_K M_{1K} \cos(\theta_{1K}) & a_K M_{2K} \cos(\theta_{2K}) & \cdots & a_K M_{NK} \cos(\theta_{NK}) \\ a_K M_{1K} \sin(\theta_{1K}) & a_K M_{2K} \sin(\theta_{2K}) & \cdots & a_K M_{NK} \sin(\theta_{NK}) \end{pmatrix} \quad (19)$$

At the same time, the Laplace transform of the output signal of Eq. (2) is as follows,

$$Y(s) = \sum_{k=1}^K b_k \left[ \cos(\phi_k) \frac{s}{s^2 + \omega_k^2} - \sin(\phi_k) \frac{\omega_k}{s^2 + \omega_k^2} \right] \quad (16)$$

Thus if the frequencies are all nonzero and different from each other, the primitives will be linearly independent and the only way two linear combinations would be the same is if all of the coefficients are equal.

The coefficients  $\tilde{\kappa}_i$  that minimize the error  $\tilde{\epsilon}_q = \|\sum_i \tilde{\kappa}_i Q_i(s) - Y(s)\|$  between the two functions in Eq. (15) and Eq. (16) are,

$$\tilde{\kappa}^* = \tilde{\Omega}_q^\dagger \mathbf{B}, \quad (17)$$

where  $\tilde{\Omega}_q$  is given by Eq. (19) and

$$\tilde{\kappa} = \begin{pmatrix} \tilde{\kappa}_1 \\ \tilde{\kappa}_2 \\ \vdots \\ \tilde{\kappa}_N \end{pmatrix} \quad \mathbf{B} = \begin{pmatrix} b_1 \cos(\phi_1) \\ b_1 \sin(\phi_1) \\ b_2 \cos(\phi_2) \\ b_2 \sin(\phi_2) \\ \vdots \\ b_K \cos(\phi_K) \\ b_K \sin(\phi_K) \end{pmatrix}. \quad (18)$$

One of the benefits of computing  $\tilde{\kappa}^*$  as opposed to computing  $\kappa^*$  is that the matrix  $\tilde{\Omega}_q$  in Eq. (19) has a number of rows equal to  $2K$ , where  $K$  is the number of frequencies, which is typically lower than the number of rows  $T$  of the matrix  $\Omega_q$  in Eq. (13). This results in lower computational cost, a simplified interpretation and analysis, and more efficient calculations. While especially useful for periodic or narrowband inputs, understanding the relationship between errors in the time and frequency domains remains essential, due to the inherently temporal nature of learning in reservoirs. Theorem 2 explicitly establishes this relationship.

**Theorem 2.** Let  $\Omega_q \in \mathbb{R}^{T \times N}$  be the reservoir state matrix of a linear decoupled reservoir computer, and let  $\mathbf{y} \in \mathbb{R}^T$  be the corresponding target output signal in the time domain. Define the time-domain readout weights  $\kappa \in \mathbb{R}^N$  as:

$$\kappa = \Omega_q^\dagger \mathbf{y},$$

where  $\Omega_q^\dagger = (\Omega_q^T \Omega_q + \beta I)^{-1} \Omega_q^T$ . Let  $\tilde{\Omega}_q$  and  $\tilde{\mathbf{y}}$  be the discrete Fourier transforms (DFT) of  $\Omega_q$  and  $\mathbf{y}$ , respectively. Then, the frequency-domain readout weights,

$$\tilde{\kappa} = \tilde{\Omega}_q^\dagger \tilde{\mathbf{y}}$$

are equal to the time-domain readout weights, i.e.,

$$\kappa \approx \tilde{\kappa}.$$

and consequently, the regression error is preserved in the two domains, i.e.,  $\tilde{\epsilon}_q \approx \epsilon_q$ .

*Proof.* The detailed proof is provided in Appendix II.  $\square$

Theorem 2 demonstrates that the error of the decoupled reservoir in the time domain is approximately equal to the error in the frequency domain. Combining the results of Theorems 1 and 2, we obtain the relations,

$$\tilde{\epsilon}_q \approx \epsilon_q \approx \epsilon_r \approx \epsilon \quad (20)$$

which shows that, regardless of whether the regression problem is posed in the coupled or decoupled form, and in the time or frequency domain, the resulting error is essentially the same.

While  $\epsilon_r$  and its frequency-domain counterpart are useful for theoretical analysis, in our numerical experiments we use the Normalized Root Mean Squared Error (NRMSE) to compare the performance of different reservoir architectures.

$$\text{NRMSE} = \frac{\|\tilde{y} - y\|}{\|y\|}, \quad (21)$$

where  $\tilde{y}$  is the approximation of the target signal,  $y$  is the true (measured or reference) signal.

## 2.2. Optimization

Having established the relationships between the errors and their formulations, we now propose an optimization framework to minimize the error of the linear reservoir computer by identifying an optimal set of eigenvalues  $\lambda_i$  in Eqs. (7) and (8). The primary goal of this procedure is to find these eigenvalues along with the parameter  $\kappa$  that jointly minimizes both the training and testing errors.

From (10) we see that each mode acts as a low-pass filter. Thus, we require the cut-off frequencies to exceed the maximum frequency present in the input signal. From Eq. (10), each mode has cut-off frequency  $\omega_{c,i} = \gamma(1 - \lambda_i)$ . Hence, we impose  $\omega_{c,i} > \omega_{\max} = \max_k \omega_k$  for all  $i$ , which yields the condition

$$\lambda_i < 1 - \frac{\omega_{\max}}{\gamma}, \quad \forall i. \quad (22)$$

Given that the input signal  $u(t)$  and the output signal  $y(t)$  are defined in Eq. (1) and Eq. (2), respectively, we now formulate the following optimization problem, incorporating the constraint in Eq. (22).

$$\min_{\lambda_1, \lambda_2, \dots, \lambda_N, \kappa} \tilde{\epsilon}_q^\top \tilde{\epsilon}_q + \beta_1 \tilde{\kappa}^\top \tilde{\kappa} + \beta_2 \left( \frac{1}{H} \right) \quad (23a)$$

$$\text{s. t. } \tilde{\epsilon}_q = \tilde{\Omega} \tilde{\kappa} - \tilde{y}, \quad (23b)$$

$$\begin{aligned} \tilde{y} = & [b_1 \cos(\phi_1), b_1 \sin(\phi_1), \\ & b_2 \cos(\phi_2), b_2 \sin(\phi_2), \dots, \\ & b_K \cos(\phi_K), b_K \sin(\phi_K)]^\top, \end{aligned} \quad (23c)$$

$$\tilde{\Omega} = \tilde{\Omega}_q, \quad (23d)$$

$$M_{ik} = \left| \frac{\gamma c_i}{j\omega_k - \gamma(\lambda_i - 1)} \right|, \quad (23e)$$

$$\theta_{ik} = \angle \frac{\gamma c_i}{j\omega_k - \gamma(\lambda_i - 1)}, \quad (23f)$$

$$\lambda_i \leq 0, \quad (23g)$$

$$H = \frac{N}{\sum_{\substack{j,z=1 \\ j \neq z}}^N \frac{1}{|\lambda_j - \lambda_z|}} \quad (23h)$$

$$\omega_{\max} + \gamma(\lambda_i - 1) \leq 0 \quad (23i)$$

In the optimization, it is desired that the eigenvalues be distinct, as this prevents dynamic degeneracy, allowing the reservoir to generate richer and more diverse responses to inputs. The cost function Eq. (23a) includes three terms. The first term represents the reservoir's error in the frequency domain and serves as the primary quantity to be minimized. High output readouts often indicate overfitting and can amplify noise in the reservoir states or inputs, leading to poor generalization and reduced robustness. To mitigate this, a second term is included in the cost function

that minimizes the norm of the output readouts, where  $\kappa$  is the vector of output readout weights, and  $\beta_1$  is a positive constant controlling the weight of this penalty. The third term is the reciprocal of the harmonic mean of the differences between the eigenvalues, which is lower when the difference in eigenvalues is high. It is included in the cost function to enforce distinctness among the eigenvalues, and  $\beta_2$  is the weight that controls the strength of this term.

### 3. Numerical Verifications

We validate the theoretical results through numerical simulations. Reservoir computer simulations are carried out in both MATLAB and Julia. The optimization problem is numerically solved using Ipopt, a nonlinear optimization solver, in combination with the JuMP modeling framework in Julia, following Algorithm 1. The procedure in the Algorithm 1 is repeated with different initial values for  $\lambda_0$ , which have been chosen from a uniform distribution over the interval  $[-20, 0]$ , and the best performance is stored as the optimal solution. The vector  $\kappa_0$  is then obtained using ridge regression, while  $M_0$ , and  $\theta_0$  are computed according to Eq. (12). (The implementation code is publicly available at [here](#))

---

#### Algorithm 1 Reservoir Eigenvalue Optimization

---

**Input:**  $N, K, \beta_1, \beta_2, \gamma, \mathbf{a}, \mathbf{b}, \Phi, \omega, \mathbf{c}, \lambda_0, \kappa_0, M_0, \theta_0$

**Output:** Optimized  $\lambda, \kappa, M, \theta$ , lowest\_error

```

1: warm_start  $\leftarrow 50$ 
2:  $\mathbf{W} \leftarrow \frac{1}{\omega}$ 
3: lowest_error  $\leftarrow \infty$ 
4: num_iter  $\leftarrow \text{warm\_start}$ 
5: for iter = 1 to num_iter do
6:   Cost =  $\min \sum_{i=1}^K W_i(\epsilon_{\cos,i}^2 + \epsilon_{\sin,i}^2) + \beta_1 \sum_{j=1}^N \kappa_j^2 + \beta_2(1/H)$ 
7:   Add nonlinear constraints
8:   Set initial values for  $\lambda, \kappa, M, \theta$  from the previous iteration or initial guess.
9:   Solve the optimization problem and find  $\lambda_{\text{new}}, \kappa_{\text{new}}, M_{\text{new}}, \theta_{\text{new}}$ 
10:  if solver converged successfully then
11:     $\epsilon = \sqrt{\sum_i W_i(\epsilon_{\cos,i}^2 + \epsilon_{\sin,i}^2)}$ 
12:    if  $\epsilon < \text{lowest\_error}$  then
13:      lowest_error  $\leftarrow \epsilon$ 
14:      Store current  $\lambda_{\text{new}}, \kappa_{\text{new}}, M_{\text{new}}, \theta_{\text{new}}$  as the best solution.
15:    end if
16:  else
17:    Keep previous  $\lambda_{\text{best}}, \kappa_{\text{best}}, M_{\text{best}}, \theta_{\text{best}}$  as the current solution.
18:  end if
19: end for
20: return  $\lambda_{\text{best}}, \kappa_{\text{best}}, M_{\text{best}}, \theta_{\text{best}}, \text{lowest\_error}$ 

```

---

#### 3.1. Optimal Reservoir Computer

To demonstrate the effectiveness of the proposed optimization framework, two numerical examples are considered involving a reservoir computer governed by Eq. (3): one with  $N = 10$  nodes and the other with  $N = 100$  nodes. In both examples, the reservoir is trained for 3000 steps with parameters  $\beta_1 = 10^{-7}$ ,  $\beta_2 = 10^{-1}$ , and  $\gamma = 6$ , and the reservoir states together with the corresponding errors are computed using both analytical and numerical methods. The matrix  $A$  is taken to be the adjacency matrix of a weighted/unweighted Erdos-Renyi graph with its spectrum shifted to ensure the Hurwitz property, and the input mask vector  $c$  has entries randomly drawn from a normal distribution. The input and output signals are defined as follows:

$$u(t) = 1.1 \cos(t) + 1.7 \cos(3t) + 2.1 \cos(5t)$$

$$y(t) = 2.2 \cos(t - 0.5) + \cos(3t + 0.9) + 1.6 \cos(5t + 1.1).$$

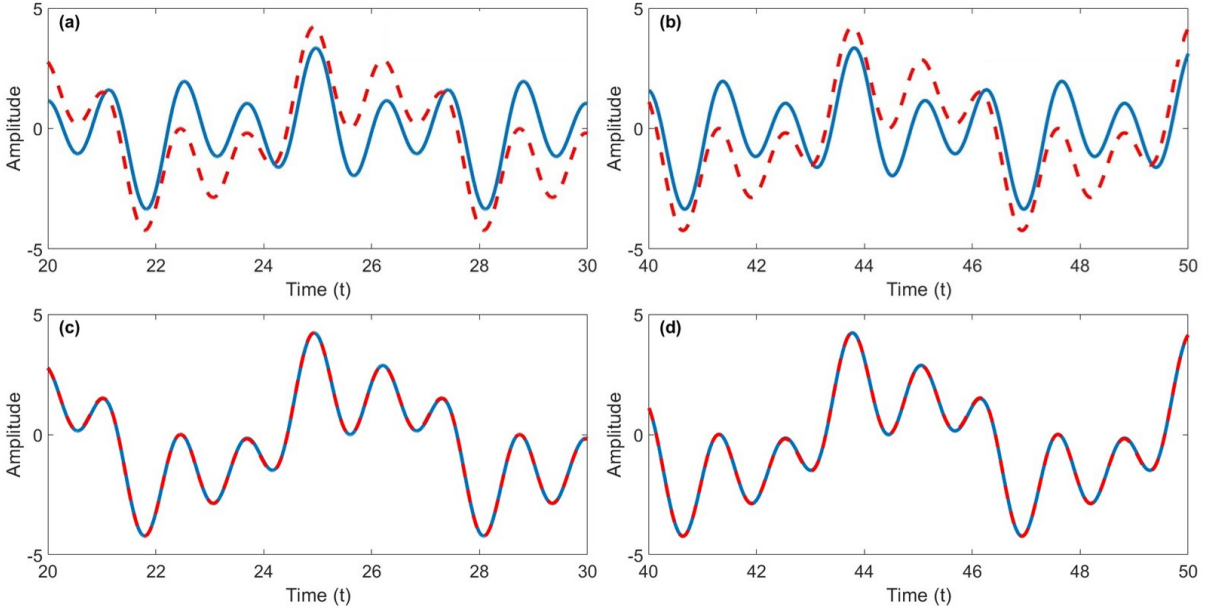


Figure 2: Performance of the 10-node reservoir. Red dashed lines represent the input signal, while blue lines correspond to the reservoir computer output: (a) Training before optimization, (b) Testing before optimization, (c) Training after optimization, (d) Testing after optimization.

The reservoir states and their corresponding prediction errors are computed both prior to and following the optimization process. By comparing the pre- and post-optimization results, we assess whether the optimization successfully reduced the observation error.

Figure (2) demonstrates the performance of the reservoir computer in the training and testing phases, respectively, before and after the optimization. As shown in the figure, prior to optimization, the reservoir was unable to learn the underlying structure of the signal resulting in a large approximation error. In contrast, after the optimization, the reservoir successfully captured the signal dynamics and reproduced the target output with significantly improved accuracy.

The optimization formulation is also effective for larger networks. Figure (3) illustrates the reservoir's performance before and after the optimization for a  $N = 100$ -node network. According to the Figures (2) and (3), the proposed optimization shows significant potential for improving signal estimation accuracy.

### 3.2. Performance Relative to Existing Approaches

To evaluate the performance of the proposed optimal LRC, it is compared with a benchmark nonlinear reservoir computer reported in Gauthier et al. (2021), using two activation functions: “tanh” and “ReLU”, as well as with a linear reservoir computer benchmark. Fig. (4) presents the training NRMSE of the optimized reservoir alongside the three benchmarks under two scenarios. In the first scenario, the number of reservoir nodes is fixed at 50 while the number of input frequencies varies; in the second, the number of input frequencies is fixed at 3 while the number of reservoir nodes varies. These cases allow assessment of the impact of network size and input complexity on performance and highlight the advantages of the proposed optimal reservoirs over the benchmarks.

Figure (4)(a) shows that the optimized LRC achieves the lowest training error, while the linear benchmark exhibits the highest. The NLRC with tanh activation performs better than the optimized LRC when the number of input frequencies is small; however, its error increases sharply as the frequency count grows, eventually exceeding that of the optimized LRC. In contrast, the optimized LRC shows only a modest increase in error under the same conditions, demonstrating greater robustness to input complexity and stronger generalization than the other methods. The NLRC with ReLU activation performs worse than the tanh-based reservoir but still outperforms the linear benchmark.

Figure (4)(b) shows that the optimized LRC achieves the lowest NRMSE when the reservoir size is small. As the number of nodes increases, however, the NRMSE of the tanh-based NLRC decreases drastically, eventually surpass-

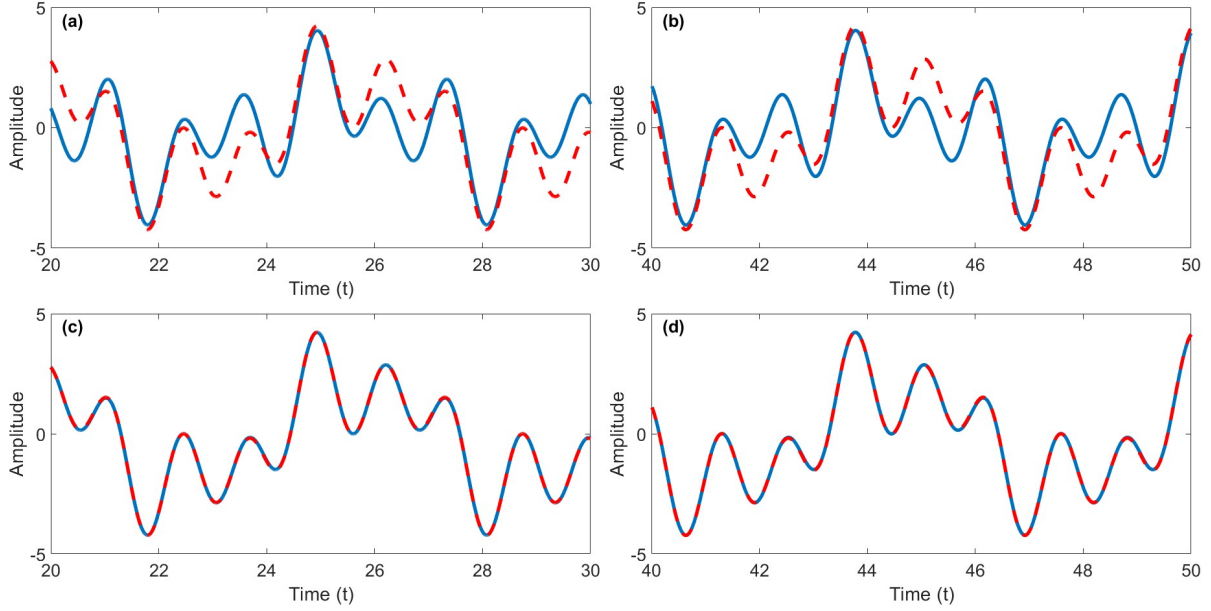


Figure 3: Performance of the 100-node reservoir. Red dashed lines represent the input signal, while blue lines correspond to the reservoir computer output: (a) Training before optimization, (b) Testing before optimization, (c) Training after optimization, (d) Testing after optimization.

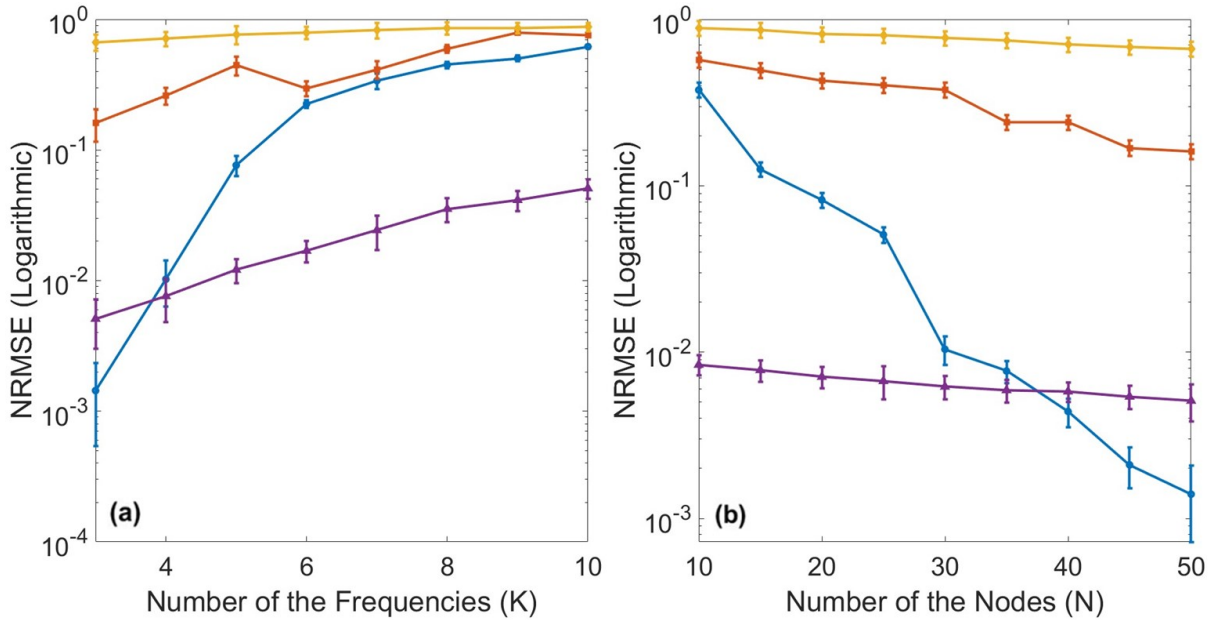


Figure 4: Average normalized root mean squared error (NRMSE) of reservoir computers with their corresponding standard deviations. The yellow line represents the NRMSE of the linear benchmark, the orange line corresponds to the NLRC with ReLU activation, the blue line shows the NLRC with tanh activation, and the purple line indicates the optimized reservoir computer. a) The number of nodes is fixed at 50 while the number of input frequencies increases. b) The number of input frequencies is fixed at 3 while the number of reservoir nodes increases.

ing the optimized LRC, while the linear benchmark maintains the highest NRMSE with only minor improvements. The ReLU-based NLRC exhibits consistently higher errors than both the optimized LRC and the  $\tanh$ -based NLRC, with only gradual reduction as the number of nodes increases. Importantly, the optimized LRC achieves significantly lower NRMSE with far fewer nodes compared to the  $\tanh$ -based NLRC. This reduction in required network size directly translates into lower computational cost, making the proposed optimized LRC more efficient for real-time and resource-constrained applications.

### 3.3. Effect of the Cost Function Components on the Optimization Performance

The optimization formulation, as shown in Eq. (23), consists of three terms. The second and third terms have associated weights  $\beta_1$  and  $\beta_2$ , respectively. Therefore, it is important to analyze the impact of these coefficients on the overall optimization process. Figure (5) (a) demonstrates the effect of the second and third terms' weights on the optimization of the error.

Figure (5) (a), shows that reducing the weight of the second term ( $\beta_1$ ) leads to a decrease in optimization error. This suggests that allowing larger output weights enables the reservoir to more effectively learn the signal, thereby improving performance. Additionally, increasing the weight of the third term ( $\beta_2$ ) also leads to a reduction in error. This is because the third term encourages the optimization to produce distinct eigenvalues, which is a desirable property.

### 3.4. Effect of $\lambda$ on Reservoir Performance

Performing a sensitivity analysis of the reservoir's eigenvalues is important for assessing both robustness and generalization. High sensitivity means that small perturbations in eigenvalues can lead to large errors, making the system fragile. It may also indicate overfitting, where the reservoir performs well only under narrowly tuned conditions. Evaluating sensitivity helps ensure stable and reliable performance. Since the optimization formulation focuses on minimizing the error by tuning the reservoir's eigenvalues and output weights, it is essential to understand how sensitive the reservoir computer is to the selection of these optimal eigenvalues. In order to do the sensitivity analysis, a small perturbation according to Eq.(24) is added to the eigenvalues.

$$\lambda_{\text{perturbed}} = \lambda_{\text{opt}} + \epsilon_s \delta, \quad \delta \in (-1, 0) \quad (24)$$

Figure (5) (b) indicates that the reservoir computer's learning error remains largely unaffected by small perturbations in the optimal eigenvalues. Only significant deviations from these optimal values cause noticeable increases in the error. This behavior suggests that the reservoir is robust and stable around the optimized eigenvalues, making it resilient to minor noise or implementation inaccuracies. Consequently, the optimized reservoir parameters provide a reliable solution, ensuring consistent performance even when slight variations occur in practice.

## 4. Conclusion

There are two main contributions of this work. First, we demonstrate that the dynamics of a linear RC can be decoupled into a number of independent modes while preserving a comparable error to the coupled RC. Second, we show that each of these modes can be individually optimized to perform a given task of interest when the decoupled RC is reformulated from the time domain into the frequency domain. This reformulation allows the reservoir modes matrix to be significantly reduced, since the number of input frequencies is typically much smaller than the number of time steps. We show that the effect of the connectivity of the reservoir on the training and testing error is completely captured by the eigenvalues of the reservoir adjacency matrix, which allows us to formulate an optimization problem in the eigenvalues only. Simulations on networks of varying sizes demonstrate that the optimized RC significantly outperforms randomly constructed reservoirs in both the training and testing phases. Moreover, comparisons with established reservoir computing benchmarks indicate that the optimized reservoir not only achieves superior performance but also exhibits greater robustness to input complexity, stronger generalization capabilities, and higher efficiency for real-time and resource-constrained applications.

## Acknowledgement

We would like to acknowledge generous help from Dr. Saif R. Kazi and Dr. Amir Nazerian.

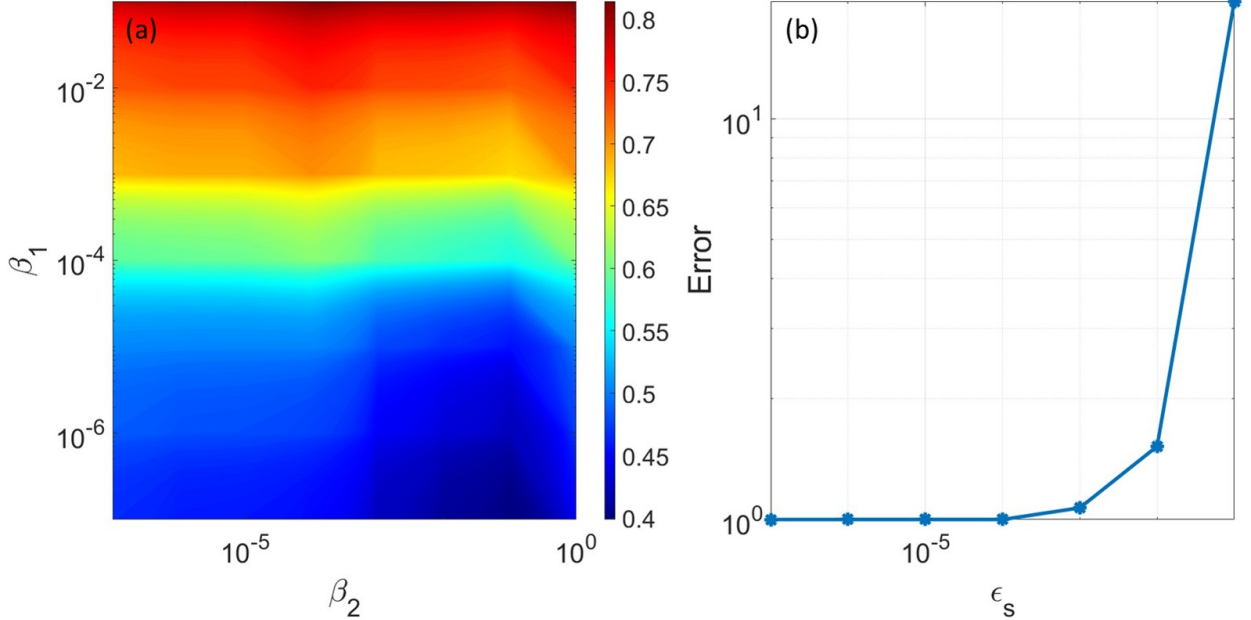


Figure 5: a) Effect of optimization terms' weights on the optimization error. b) Sensitivity of the Reservoir Training Error to Optimal Eigenvalues.

### Appendix A. Proof of Theorem I

A coupled and a decoupled linear reservoir are described by Eqs. (3) and (7), respectively. We now consider the two regression problems, one for coupled modes and the other for decoupled modes with fit signals,

$$h_r(t) = \sum_j \kappa_j r_j(t) + \kappa_{N+1}, \quad (\text{A.1})$$

$$h_q(t) = \sum_j \kappa'_j q_j(t) + \kappa'_{N+1}. \quad (\text{A.2})$$

The best fit signals are the same,

$$h_q(t) = h_r(t) = h(t), \quad (\text{A.3})$$

Imagine solving the first regression problem and finding the coefficients  $\kappa_1^*, \kappa_2^*, \dots, \kappa_N^*, \kappa_{N+1}^*$  that minimize the error between  $h_r(t)$  and the output signal  $y(t)$ . Then we rewrite Eq. (A.2),

$$h(t) = \sum_j \kappa'_j \sum_k V_{kj} r_k(t) + \kappa'_{N+1} + \sum_k \left( \sum_j V_{kj} \kappa'_j \right) r_k(t) + \kappa'_{N+1} \quad (\text{A.4})$$

By comparing Eqs. (A.1) and (A.4) in the same signals  $r(t)$ , one immediately sees that they must admit optimal solutions such that the  $N$  dimensional vectors,

$$\kappa^* = V \kappa'^* \quad (\text{A.5})$$

and

$$\kappa'^*_{N+1} = \kappa^*_{N+1}. \quad (\text{A.6})$$

The training and testing errors remain the same because the transformation is invertible and preserves the linear span of the feature space, ensuring that the mapping between the input and output signals is unchanged.

## Appendix B. Proof of Theorem II

For sufficiently large  $t$ , the Eq. 11 and Eq. 2 can be expressed as

$$q_i(t) = \sum_{k=1}^K a_k M_{ik} [\cos(\omega_k t) \cos(\theta_{ik}) - \sin(\omega_k t) \sin(\theta_{ik})], \quad (\text{B.1})$$

$$y(t) = \sum_{k=1}^K b_k [\cos(\omega_k t) \cos(\varphi_k) - \sin(\omega_k t) \sin(\varphi_k)]. \quad (\text{B.2})$$

The optimal solution of the time-domain regression is

$$\boldsymbol{\kappa}^* = \Omega_q^\dagger \mathbf{y}, \quad \Omega_q^\dagger = (\Omega_q^T \Omega_q + \beta I)^{-1} \Omega_q^T. \quad (\text{B.3})$$

where  $\Omega_q$  is the matrix of the decoupled reservoir states in the time domain. Taking the Fourier transform gives

$$\mathcal{F}[q_i(t)] = \sum_{k=1}^K a_k M_{ik} [\pi \cos(\theta_{ik}) (\delta_{\omega_k} + \delta_{-\omega_k}) + \pi j \sin(\theta_{ik}) (\delta_{\omega_k} - \delta_{-\omega_k})] \quad (\text{B.4})$$

$$\mathcal{F}[y(t)] = \sum_{k=1}^K b_k [\pi \cos(\phi_k) (\delta_{\omega_k} + \delta_{-\omega_k}) + \pi j \sin(\phi_k) (\delta_{\omega_k} - \delta_{-\omega_k})] \quad (\text{B.5})$$

The frequency-domain regression problem is

$$\sum_i \tilde{\kappa}_i \mathcal{F}[q_i(t)] \approx \mathcal{F}[y(t)], \quad (\text{B.6})$$

which leads to

$$\sum_i \tilde{\kappa}_i a_k M_{ik} \cos(\theta_{ik}) \approx b_k \cos(\varphi_k), \quad (\text{B.7})$$

$$\sum_i \tilde{\kappa}_i a_k M_{ik} \sin(\theta_{ik}) \approx b_k \sin(\varphi_k), \quad k = 1, \dots, K. \quad (\text{B.8})$$

Solving yields

$$\tilde{\boldsymbol{\kappa}}^* = \tilde{\Omega}_q^\dagger \tilde{\mathbf{y}}. \quad (\text{B.9})$$

Since the Fourier transform is linear, invertible, and energy-preserving, there exists a one-to-one mapping between  $\boldsymbol{\kappa}^*$  and  $\tilde{\boldsymbol{\kappa}}^*$ . Thus,

$$\tilde{\boldsymbol{\kappa}}^* \approx \boldsymbol{\kappa}^*, \quad (\text{B.10})$$

and the regression error is identical in both domains, i.e.,  $\epsilon_F = \epsilon_r$ .

## References

Alain Bensoussan, Yiqun Li, Dinh Phan Cao Nguyen, Minh-Binh Tran, Sheung Chi Phillip Yam, and Xiang Zhou. Chapter 16 - machine learning and control theory. In Emmanuel Trélat and Enrique Zuazua, editors, *Numerical Control: Part A*, volume 23 of *Handbook of Numerical Analysis*, pages 531–558. Elsevier, 2022. doi: <https://doi.org/10.1016/bs.hna.2021.12.016>. URL <https://www.sciencedirect.com/science/article/pii/S1570865921000314>.

Lorenz Butschek, Akram Akrout, Evangelia Dimitriadou, Alessandro Lupo, Marc Haelterman, and Serge Massar. Photonic reservoir computer based on frequency multiplexing. *Opt. Lett.*, 47(4):782–785, Feb 2022. doi: 10.1364/OL.451087. URL <https://opg.optica.org/ol/abstract.cfm?URI=ol-47-4-782>.

Matthew Dale, Simon O’Keefe, Angelika Sebald, Susan Stepney, and Martin A. Trefzer. Reservoir computing quality: connectivity and topology. *Natural Computing*, 20(2):205–216, 2021. ISSN 1572-9796. doi: 10.1007/s11047-020-09823-1. URL <https://doi.org/10.1007/s11047-020-09823-1>.

Daniel J. Gauthier, Erik Boltt, Aaron Griffith, and Wendson A. S. Barbosa. Next generation reservoir computing. *Nature Communications*, 12(1):5564, September 2021. ISSN 2041-1723. doi: 10.1038/s41467-021-25801-2. URL <https://doi.org/10.1038/s41467-021-25801-2>.

Arash Hashemi, Grzegorz Orzechowski, Aki Mikkola, and John McPhee. Multibody dynamics and control using machine learning. *Multibody System Dynamics*, 58(3):397–431, 2023. ISSN 1573-272X. doi: 10.1007/s11044-023-09884-x. URL <https://doi.org/10.1007/s11044-023-09884-x>.

Herbert Jaeger. The “echo state” approach to analysing and training recurrent neural networks-with an erratum note. *Bonn, Germany: German National Research Center for Information Technology GMD Technical Report*, 148(34):13, 2001.

Jean Panaioti Jordanou, Eric Aislan Antonelo, and Eduardo Camponogara. Echo state networks for practical nonlinear model predictive control of unknown dynamic systems. *IEEE Transactions on Neural Networks and Learning Systems*, 33(6):2615–2629, 2022. doi: 10.1109/TNNLS.2021.3136357.

Zhixin Lu, Jaideep Pathak, Brian Hunt, Michelle Girvan, Roger Brockett, and Edward Ott. Reservoir observers: Model-free inference of unmeasured variables in chaotic systems. *Chaos: An Interdisciplinary Journal of Nonlinear Science*, 27(4):041102, 04 2017. ISSN 1054-1500. doi: 10.1063/1.4979665. URL <https://doi.org/10.1063/1.4979665>.

Michael McCreesh and Jorge Cortés. Control of linear-threshold brain networks via reservoir computing. *IEEE Open Journal of Control Systems*, 3:325–341, 2024. doi: 10.1109/OJCSYS.2024.3451889.

Claus Metzner, Achim Schilling, Andreas Maier, and Patrick Krauss. Nonlinear neural dynamics and classification accuracy in reservoir computing. *Neural Computation*, 37(8):1469–1504, 07 2025. ISSN 0899-7667. doi: 10.1162/neco\_a\_01770. URL [https://doi.org/10.1162/neco\\_a\\_01770](https://doi.org/10.1162/neco_a_01770).

Jaideep Pathak, Brian Hunt, Michelle Girvan, Zhixin Lu, and Edward Ott. Model-free prediction of large spatiotemporally chaotic systems from data: A reservoir computing approach. *Phys. Rev. Lett.*, 120:024102, Jan 2018. doi: 10.1103/PhysRevLett.120.024102. URL <https://link.aps.org/doi/10.1103/PhysRevLett.120.024102>.

Junyi Shen, Tetsuro Miyazaki, and Kenji Kawashima. Control pneumatic soft bending actuator with feedforward hysteresis compensation by pneumatic physical reservoir computing. *IEEE Robotics and Automation Letters*, 10(2):1664–1671, 2025. doi: 10.1109/LRA.2024.3523229.

Shuhei Sugiura, Ryo Ariizumi, Toru Asai, and Shun-Ichi Azuma. Nonessentiality of reservoir’s fading memory for universality of reservoir computing. *IEEE Transactions on Neural Networks and Learning Systems*, 35(11):16801–16815, 2024. doi: 10.1109/TNNLS.2023.3298013.

Francis Wyffels, Benjamin Schrauwen, and Dirk Stroobandt. *Stable Output Feedback in Reservoir Computing Using Ridge Regression*. Springer Berlin Heidelberg, Berlin, Heidelberg, 2008. ISBN 978-3-540-87536-9.

Min Yan, Can Huang, Peter Bienstman, Peter Tino, Wei Lin, and Jie Sun. Emerging opportunities and challenges for the future of reservoir computing. *Nature Communications*, 15(1):2056, 2024. ISSN 2041-1723. doi: 10.1038/s41467-024-45187-1. URL <https://doi.org/10.1038/s41467-024-45187-1>.

Xiaoning Zhao, Yougang Sun, Yanmin Li, Ning Jia, and Junqi Xu. Applications of machine learning in real-time control systems: a review. *Measurement Science and Technology*, 36(1):012003, nov 2024. doi: 10.1088/1361-6501/ad8947. URL <https://dx.doi.org/10.1088/1361-6501/ad8947>.